ELSEVIER

Dyes and Pigments 47 (2000) 53–64

DYES and PIGMENTS

www.elsevier.com/locate/dyepig

Molecular modeling of Congo Red analogues containing terphenyl and quarterphenyl moieties

Jason Lye [a], Harold S. Freeman [a,*], Russell D. Cox [b]

[a] *College of Textiles, North Carolina State University, Box 8301, Raleigh, NC 27695- 8301, USA*
[b] *Deptartment of Colour Chemistry, University of Leeds, Leeds LS2 9JT, UK*

Received 12 January 2000; accepted 14 February 2000

Dedicated to Dr. A.T. Peters

Abstract

The molecular structures of Congo Red and its terphenyl and quarterphenyl analogues were optimized by applying AM1 and PM3 semiempirical methods to partially optimized starting structures. It was necessary to carry out repetitive sequences consisting of manual adjustments to the input structures followed by optimization, in order to locate minima in each structure. In addition, the conformational space associated with rotations about the central phenyl rings was explored. AM1 predicted non-planar biphenyl, terphenyl, and quarterphenyl structures, whereas PM3 predicted planar structures. Both methods were in agreement with experimental data, in that the differences in the energy of planar and non-planar structures were small. PISYSTEM predicted that increasing the number of central phenyl rings in Congo Red would have a hypsochromic and hyperchromic effect on the absorption maximum.

Keywords: Molecular modeling; 4,4″-Diaminoterphenyl; 4,4″-Diaminoquarterphenyl; Congo Red analogs; Geometry optimization

1. Introduction

Congo Red (CI Direct Red 28, **1**) is a sulfonated azo dye that finds use today principally as a histological stain for amyloid proteins. Discovered by Böttiger in 1884 [1], the linear geometry of **1** imparts substantivity for cellulose, and it is the first dye for cotton that could be applied without using a mordant. Unfortunately, it is also known to be mutagenic in the preincubation assay [2]. The mutagenicity of Congo Red has been attributed to the generation of benzidine, via metabolic activation, a compound that is known to cause bladder cancer in humans [2,3]. In this regard, intestinal microfloral azoreductases reduce the azo nitrogens to amino groups, thus generating benzidine (2) in vivo [4–6].

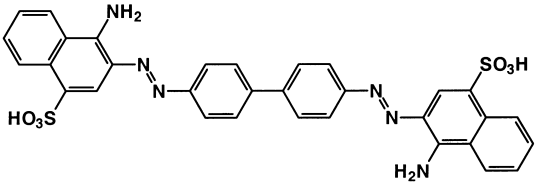

1

More recently, the ability of Congo Red to bind to amyloid proteins associated with viral recognition and replication has led to its examination as a potential HIV-1 protease and reverse tran-

* Corresponding author. Tel.: +1-919-515-6552; fax: +1-919-515-6532.
E-mail address: harold_freeman@ncsu.edu (H.S. Freeman).

0143-7208/00/$ - see front matter
PII: S0143-7208(00)00063-2

scriptase inhibitor [7,8]. The range of biological substrates to which the dye will bind has also generated interest in other areas of pharmacophore design, including the design of drugs intended for use against diseases such as spongiform encephalopathies and neurodegenerative disorders such as Alzheimer's disease [9,10].

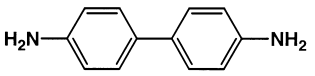

2

It appears that the potentially useful amyloid protein binding properties of Congo Red and other benzidine based dyes, such as Evans Blue and Chicago Blue 6B have been attributed to (a) the symmetrical structures of such molecules and (b) the separation of negatively charged groups [11]. These two factors enable the dye to intercalate at the interface of two globular porcine insulin molecules [11]. Similarly, binding to HIV-1 protease is thought to take place via dye–enzyme interactions between hydrophilic, positively charged arginine residues located on each side of a symmetric substrate binding cavity [8]. Thus, Congo Red is an important lead structure in the development of certain pharmaceuticals.

Unfortunately, the beneficial properties that the benzidine moiety imparts to dyes and potential xenobiotics cannot be exploited until the toxicity of the benzidine moiety can be reduced. Efforts directed towards the development of non-mutagenic analogues of dyes based on benzidine have previously included (a) the examination of 5,5′-diamino-2, 2′-bipyridyl as a non-mutagenic tetra-zotizable replacement for benzidine [3,12], and (b) incorporating bulky groups (R) in the 3, 3′-positions on the benzidine moiety, to give dyes such as **3** [12].

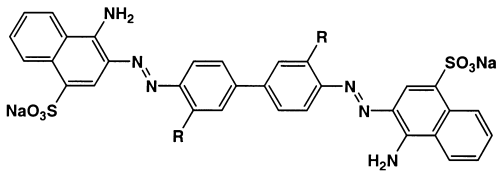

3 (R = OPr, Pr)

The present investigation focuses on the molecular modeling of Congo Red analogues that are based on 4,4″-diaminoterphenyl (**4**) and 4,4‴-diaminoquarterphenyl (**5**). It was anticipated that the introduction of the third and fourth phenyl rings into dye structures based on *para*, *para*′-diaminooligobiphenyls would reduce mutagenicity, while retaining the desirable substantivity for cellulose that characterizes a benzidine (diaminobiphenyl) moiety.

As part of ongoing investigations into the applicability of molecular modeling for the design and synthesis of novel dyes, we sought to test our molecular modeling systems by applying them to Congo Red as well as the terphenyl and quarterphenyl analogues. We were particularly interested in the predicted conformation of the central phenyl rings with respect to the rest of the molecule.

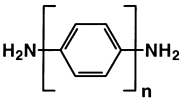

4. n=3, **5**. n=4

It appears from X-ray crystallography that the barrier to mutual rotation of the two symmetrical halves of Congo Red is low enough that two conformers (one twisted about the central phenyl–phenyl bond and one planar) co-crystallize as the Ca^{2+} salt, although it should be pointed out that the effect of the Ca^{2+} in close proximity to the chromogen is not known [13]. The non-planar form of the dye had a dihedral angle between the two phenyl rings of 25° in the crystal, and the sulfonate groups were oriented *anti* with respect to the long axis of the molecule in both the planar and non-planar forms [13].

Also, extensive experimental data are available concerning conformations of biphenyl and biphenyl derivatives. Observations of rotational overtones using vapor phase Raman spectroscopy were used to determine the phenyl-phenyl dihedral angle to be 45° and the energy barrier to rotation about the phenyl-phenyl bond to be 1.43 kcal mol^{-1} [14]. Electron diffraction experiments later showed that in the vapor phase, the dihedral angle was 44.4–46.8°, and that energy maxima were only 1.43 kcal mol^{-1} in the case of the planar rotamer and 1.55

kcal mol^{-1} in the case of the perpendicular rotamer [15]. Interestingly, although the effect of substituents in positions 3, 4 and 5 on the energy barriers to rotation were small, deuterated biphenyl was found to have slightly higher energy planar and perpendicular conformers (2.37 and 2.20 kcal mol^{-1}, respectively).

X-ray studies at 110 K [16] and at 293 K [17] showed that biphenyl adopted a planar conformation in the crystal lattice. Brock and Minton [18] compiled X-ray data for 101 biphenyl derivatives that contained hydrogen atoms in all four *ortho* positions in order to study the effect of crystal forces on biphenyls. The authors concluded that (a) although experimental data showed non-planar minima in the vapor phase, solid phase biphenyls often existed as planar molecules, and (b) the central phenyl–phenyl bond length was independent of the dihedral angle between the two rings. The authors also found that thermal motion in the long axis of the molecule was greater in cases involving planar molecules, and suggested that the increased thermal freedom in this direction helped to stabilize the planar form of biphenyl in the crystal lattice [18].

X-ray crystal data are also available for terphenyl and quarterphenyl, and neutron diffraction data are also published for the former [19–21]. Terphenyl is an essentially planar molecule, although the central phenyl ring has more than one possible conformation [19–21]. At room temperature, the central phenyl ring oscillates between two degenerate minima, by rotation through 13.3° either side of the molecular plane [20, 21]. Neutron diffraction data suggest that the energy barrier between the two minima is 0.6 kcal mol^{-1} [20]. The X-ray crystal structure of *para*-quarterphenyl has been determined at room temperature and this structure is also essentially planar [22]. However, investigators reported unusually large thermal motion in the central phenyl rings, and this effect was attributed to the central rings oscillating between two minima, which lay at approximately 11° either side of the mean molecular plane [22].

Previous attempts to model biphenyl using all-valence semiempirical methods (e.g. CNDO/2 [23] and INDO [24]) met with limited success. The correlation between predicted and experimental data concerning the conformational analysis of biphenyl was improved when extra terms were introduced into a modified INDO approach, allowing interactions between the $\pi\pi$ and $\sigma\sigma$ electron systems to be considered [24]. Recent ab initio modeling studies carried out at HF/6-31G* and HF/6-31G** levels afforded good agreement with vapor-phase experimental data concerning the predicted equilibrium geometry of biphenyl, although the energy of the planar geometry was predicted to be more than double the experimental value [25]. Also, in contrast to experimental (electron diffraction) data, the perpendicular geometry was predicted to be lower in energy to the planar geometry. Thus, even ab initio HF/6-31G** calculations were unable to predict the internal rotation barriers of biphenyl [25]. It appears that the abilities of AM1 and PM3 to model biphenyl, or derivatives of biphenyl, such as Congo Red, have not been determined.

The semiempirical methods AM1 and PM3 provided the opportunity to conduct numerous modeling experiments on relatively large molecules using inexpensive computer hardware in a reasonable timeframe. On the other hand, *ab initio* methods require lengthy calculation times and powerful computing facilities to study large molecules. Thus, the AM1 and PM3 methods offer a useful compromise in terms of hardware demands, speed, and accuracy when investigating large molecules such as those involved in the present study. In addition, the low energy barrier to rotation about the central linear polyphenyl moiety in 1 ($n=2$), 6 ($n=3$), and 7 ($n=4$) give rise to a number of possible low energy structures. For this reason, the geometry optimization procedure used in the present study was unlike procedures previously employed in our work [26], or that of others [23–25].

2. Experimental

In order to distinguish the minima generated by rotating about the phenyl–phenyl links in **1**, **6** and **7**, it was necessary to first fully optimize the naphthylamino-azo moieties. If this was not carried out first, the large changes in energy accompanying

optimization of the naphthylamino-azo moieties tended to overshadow the small energy changes associated with rotations about the central phenyl-phenyl bonds. The procedure employed involved optimizing the structure using either AM1 or PM3 until the conjugate gradient fell below 1, then editing the molecule, by rotating about the phenyl–phenyl bonds to generate starting structures for further optimization.

The naphthylamino-azo residue of **1**, **6** and **7** has three possible rotameric arrangements. Two *anti* arrangements are shown in Fig. 1 (cf. **a** and **b**). A third possibility would consist of a mixture of **a** and **b**, in which one azo group would have the configuration shown in **a**, and the other would have the configuration of the azo groups in **b**. X-ray crystallography of the calcium salt of Congo Red indicated that rotamer **1a** was the form of lowest energy, although it is not clear how the Ca^{2+} ions contribute to the final structure. We were also interested in determining whether the modeling system used for this aspect of the investigation would predict rotamer **1a** to be the lowest energy rotamer.

Although Congo Red is usually employed as the sodium salt, for a number of reasons, the calculations were simplified by modeling the free acid structure. For instance, because single molecules of Congo Red were modeled, it was not possible to determine the precise position of counter ions with respect to the ionized dye. Counter ion positioning could introduce unnecessary errors.

2.1. Geometry optimization

Structures **1a–b** and **6–8a–b**, were built using CAChe Editor [27] and optimized using an augmented MM2 forcefield. The resultant structures were edited to make them planar, and then optimized using AM1 [28] and PM3 [29, 30], in conjunction with an eigenvector following converger. The geometry was optimized until the conjugate gradient fell below 1 in CAChe MOPAC [27]. At this stage, the central polyphenyl moiety of every partially optimized structure was non-planar. The structures were edited to make two "starting structures" for both rotamers of each compound. One starting structure was edited to make the central phenyl rings coplanar, and the other was edited so that the angle between the planes formed by each phenyl ring (the dihedral angle) was 30°. An example of a planar starting structure is shown in Fig. 2, and Fig. 3 provides an example of a non-planar starting structure.

The "starting structures" were re-optimized using MOPAC AM1 or PM3 in conjunction with an Eigenvector following energy minimizer. The keyword PRECISE was used to increase the self-consistent field convergence criterior by a factor of 10 from the default, and the structures were optimized until the conjugate gradient fell below 1. The structures were then re-edited so that the polyphenyl moieties were re-set to their starting positions (e.g. as shown in Figs. 2 and 3), and then re-submitted for optimization in MOPAC. For the

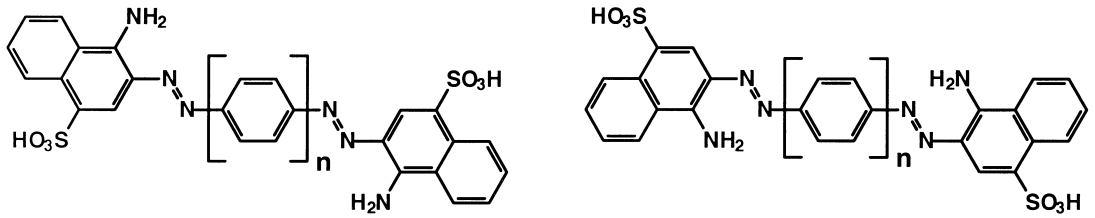

a **b**

1 (n=2), **6** (n=3), **7** (n=4), **8** (n=1)

Fig. 1. Rotamers of dye **1** and homologues **7** and **8**.

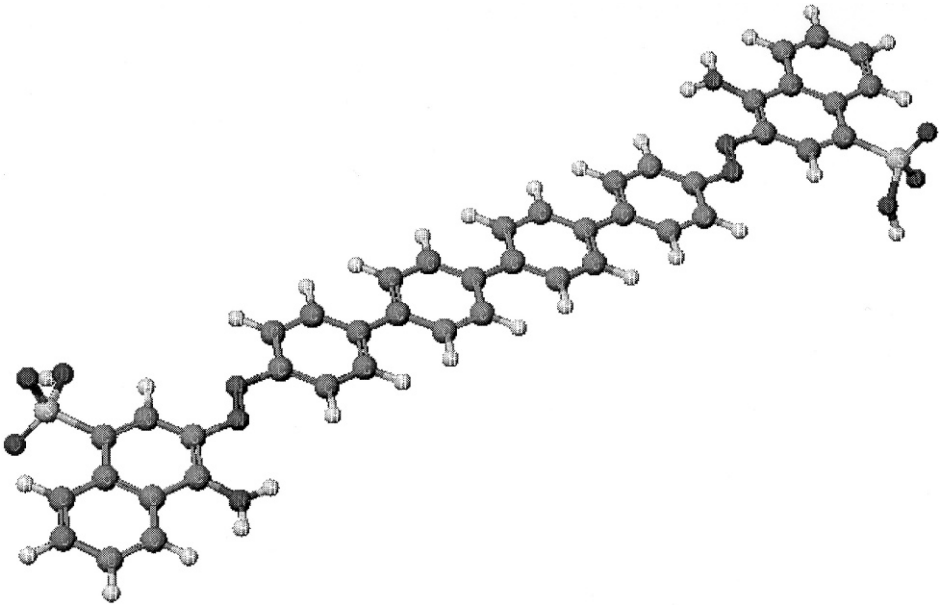

Fig. 2. The planar starting structure for dye **7**.

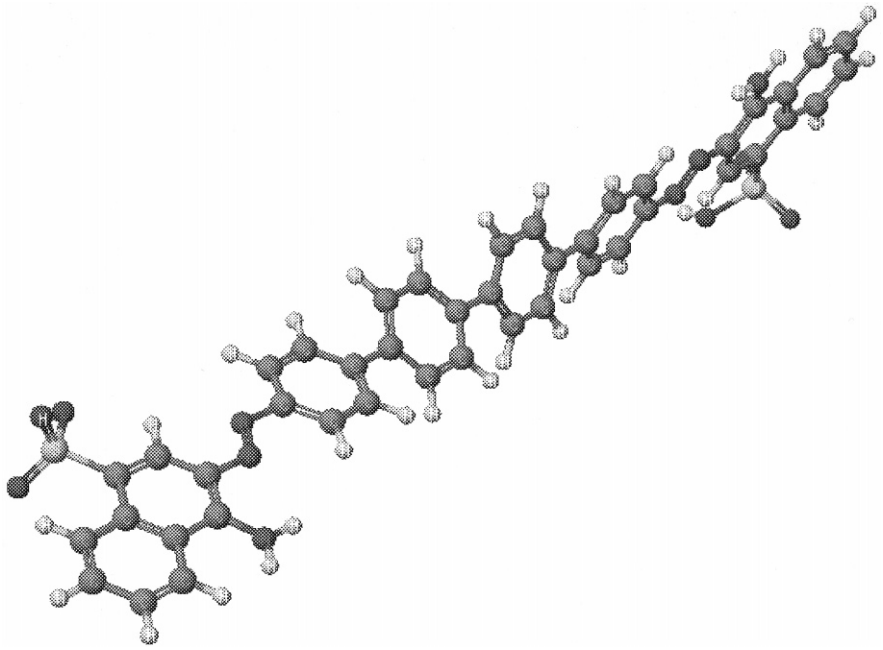

Fig. 3. A non-planar starting structure for dye **7**.

final optimizations, the keyword GNORM = 0.1 was also specified. For this reason, almost all of the optimizations were converged so that the gradient fell below 0.1 kcal $Å^{-1}$. In most cases, the geometries were resubmitted to MOPAC at least twice — the phenyl rings were re-adjusted before each resubmission. No further tests were carried out on optimized structures.

2.2. Colour prediction

CAChe Zindo [27,31,32] was used to predict state energies of planar PM3 optimized geometries in a configuration interaction (CI) calculation. The excited configuration manifold was generated using the 14 highest energy occupied MOs and the 14 lowest energy unoccupied MOs. Further increases in the manifold size did not significantly influence the predicted spectra near λ_{max}. Spectroscopic predictions using PISYSTEM [33] were based on the results of a limited CI calculation involving the 36 lowest energy singly excited configurations. PISYSTEM is a commercial package based on the PPP π-only approach [34–36].

3. Results and discussion

Tables 1 and 2 contain the calculated energy values, gradients, and phenyl-phenyl dihedral angles for optimized geometries of **1**, **6** and **7**, from AM1 and PM3 calculations. Clearly, both methods predict that rotamer **a** is always a lower energy conformer than rotamer **b**. These results are consistent with published X-ray crystallographic data [13].

Having determined that X-ray analysis and modeling data are in agreement that rotamer **a** is the lowest energy conformer for the azo-naphthionic acid segment of the 3 dyes studied, subsequent data analyses focused on structures based on this rotamer.

Table 1 shows that PM3 predicts the central phenyl rings in **1**, **6** and **7** to be co-planar. An example of a PM3-optimized structure that employed a planar starting structure is shown in Fig. 4. As expected, some pyramidalization of the amino groups occurred [26]. Dyes **6** and **7** gave similar results. Interestingly, the predicted energy difference between planar and non-planar Congo Red dye structures (i.e. 0.27 kcal mol^{-1}) was similar to that obtained for vapor phase biphenyl using electron diffraction methods (0.12 kcal mol^{-1} [15]).

PM3 geometry optimizations initiated from non-planar starting structures were interesting, because the final structures always contained at least one planar biphenyl moiety (Fig. 5). The structure of the terphenyl analogue **6** also contained a planar biphenyl moiety after optimization, as evident from the dihedral angle data in Table 3. Although the reasons for this preference are unclear, it may be due to a predicted stereoelectronic effect involving ππ-orbital overlap between adjacent phenyl rings.

On the other hand, results from AM1 suggested that **1**, **6**, and **7** would have non-planar structures in a vacuum. Calculations carried out using AM1 on non-planar starting structures gave optimized structures that were similar to starting structures of the type shown in Fig. 3.

AM1 optimizations of planar structures returned non-planar geometries, in which the

Table 1
AM1 and PM3 geometry optimization results for rotamers **a**

Starting structures	Final gradient (kcal $Å^{-1}$)		Final energy (kcal mol^{-1})		Final dihedral angle(s)	
	AM1	PM3	AM1	PM3	AM1	PM3
1a (planar)	0.094	0.088	−0.44	−16.72	39.8°	0.9°
1a (non-planar)	0.170	0.084	−0.44	−16.45	40.2°	0.9°
6a (planar)	0.098	0.094	25.80	9.27	40.6o°−39.4°	0.3°,−1.3°
6a (non-planar)	0.083	0.086	25.62	9.87	40.7°, 40.5°	0.9°, 46.9°
7a (planar)	0.296	0.085	51.54	33.01	−41.6°, 40.2°, 39.7°	0.4°,−1.1°,−0.1°
7a (non-planar)	0.449	0.440	51.63	34.02	40.4°, 39.5°, 39.2°	1.3°, 46.7°, 1.0°

dihedral angles between benzene rings were approximately 40°. Fig. 6 shows an example of the results of an AM1 optimization of a planar starting structure.

Brock and Minton [18] compiled data from 91 crystal structures of biphenyl derivatives, and found that the average phenyl–phenyl bond length was 1.484 Å, and that this value was independent of the twist angle between the two phenyl rings. Ojala et al. [13] observed two conformers of Congo Red in the same crystal, and found the phenyl–phenyl bond length to be 1.48 Å in the non-planar conformer and 1.50 Å in the planar conformer. In the present study, we found that PM3 predicted the phenyl–phenyl bond length to be 1.469 Å in both the planar and non-planar minima. AM1 predicted the bond length to be 1.461 Å in the non-planar form.

To further examine differences in the geometries predicted by AM1 and PM3, rigid conformational search maps were generated for **1** using MOPAC. The first reaction coordinate of interest involved

Table 2
AM1 and PM3 geometry optimization results for rotamer **b**

Starting structures	Final gradient (kcal Å^{-1})		Final energy (kcal mol^{-1})		Final dihedral angle(s)	
	AM1	PM3	AM1	PM3	AM1	PM3
1b (planar)	0.094	0.083	0.31	−13.36	39.3°	0.2°
1b (non-planar)	0.086	0.137	0.31	−12.75	39.9°	48°
6b (planar)	0.879	0.097	26.64	12.44	39.7°,−39.6°	2.6°, 2.3°
6b (non-planar)	0.094	0.066	26.46	13.03	39.9°, 40.0°	4.0°, 48°
7b (planar)	0.088	0.062	51.86	36.32	39.5°,−39.9°, 39.7°	0.8°, 0.6°, 0.7°
7b (non-planar)	0.407	0.086	52.17	36.97	39.8°, 39.7°, 39.5°	2.9°, 48°, 2.7°

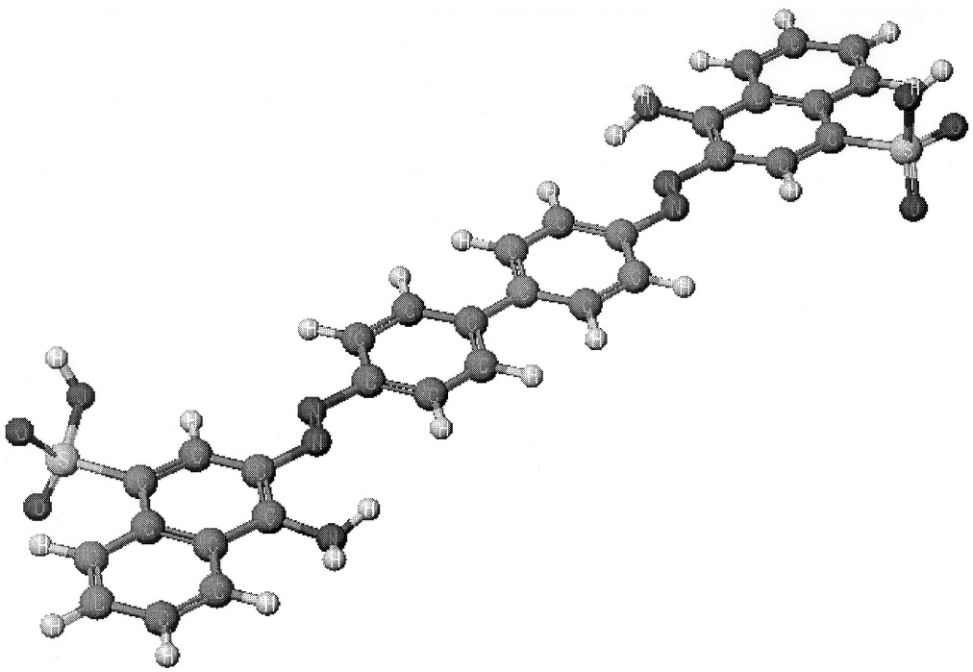

Fig. 4. PM3-optimized **1** — generated from a planar starting structure.

rotation about the central phenyl–phenyl bond of **1**; this coordinate was searched from 0 to 90° in 30 increments of 3°. The second degree of freedom explored was the length of the central phenyl–phenyl bond. As the phenyl–phenyl bond length was predicted to be 1.469 Å (PM3) in both planar and non-planar structures, this bond length was varied between 1.44 and 1.53 Å over 9 increments of 0.01 Å. Thus, 270 point energy calculations were used to construct conformational maps for **1** using AM1 and PM3. Fig. 7 shows the map calculated using PM3. Note the position of the global minimum (represented by the black ball) at planar (0°) geometry, and a local minimum at about 40°. Consequently, PM3 predicts the planar conformer of **1** to be a lower energy conformer than the perpendicular (dihedral1 = 90°) conformer. Fig. 8 shows the corresponding map from AM1 calculations. In this case, note the position of the predicted global minimum (represented by the black ball) at about 40° twist. In contrast to PM3, AM1 predicts the planar geometry to be higher in energy than

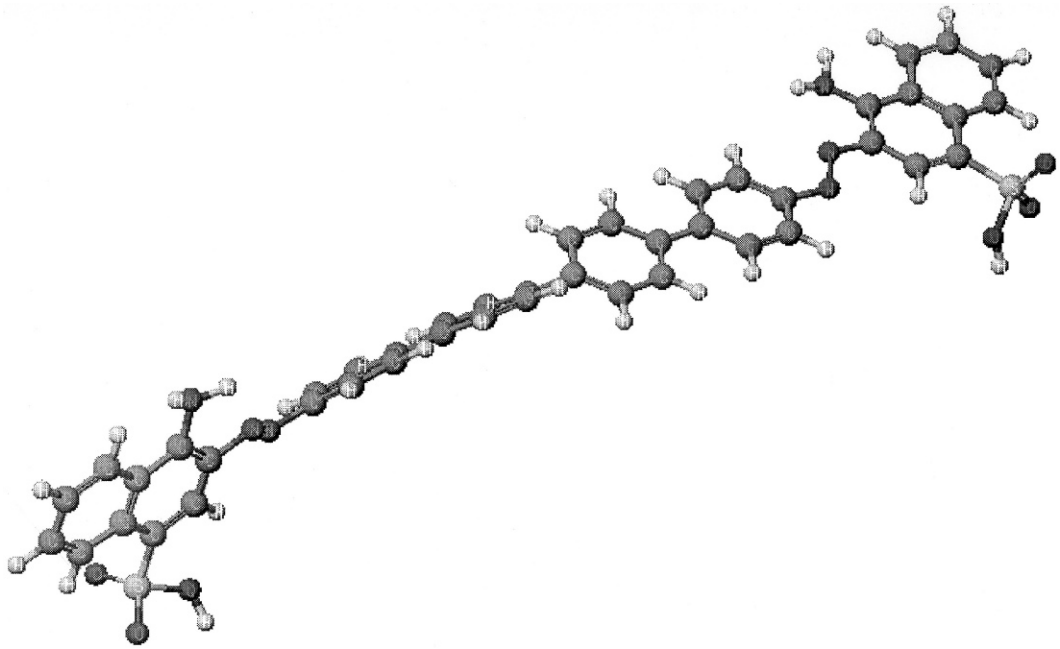

Fig. 5. PM3-optimized **7** — generated from a non-planar starting structure. Two planar biphenyl moieties are evident in this structure.

Table 3
Calculated absorption maxima and intensities for compounds 1 and 6–8

	Experimental	PISYSTEM calculations		ZINDO calculations	
Compound	λ_{max} (nm)	λ_{max} (nm)	Oscillator strength	λ_{max} (nm)	TMV (D)
1	497	493.6	1.930	381	13.283
6	–	482.4	2.154	381	14.243
7	–	479.6	2.374	383	15.614
8	–	515.5	1.667	385	11.267

the perpendicular geometry, in contrast to vapor phase experimental data. Conformational search maps were also constructed for **7**, and were found to be very similar to those shown in Figs. 7 and 8.

It is clear that PM3 and AM1 gave different results; PM3 predicted the global minimum to correspond to a planar geometry, whereas AM1 predicted planar geometry to be a high-energy form. While AM1 predicted a non-planar global minimum, a similar configuration was predicted to be a local minimum by PM3. The energy barrier to rotation between the two minima on the PM3 conformational surface was predicted to be small (<0.4 kcal mol^{-1}). However, transition state energy estimations could not be taken from rigid search maps, as they only showed the exploration of two degrees of freedom associated with the molecule. This means that they were not true saddle points.

Previously optimized structures were used to construct the rigid search maps. Accordingly, the map constructed using PM3 was initiated using a previously optimized planar structure, eliminating possible energy changes associated with mutual bending back of the *ortho* hydrogen atoms at the biphenyl linkage. In the case of AM1, the optimized structure was non-planar, and therefore mutual bending of the *ortho* hydrogen atoms at the biphenyl linkage would cause an artificially high-energy situation in planar conformers.

There are two key factors governing the conformation of the phenylene compounds in this study. The steric interaction between the hydrogen atoms of adjacent phenyl rings increases the energy of the planar conformer. However, overlap of π-orbitals on adjacent rings tends to stabilize the planar conformation. It has been suggested that AM1 tends to slightly underestimate ππ-system resonance energy [37], which may account in part for the reason AM1 favors the non-planar conformers of **1, 6** and **7**. It has also been suggested that PM3 does not correctly account for steric

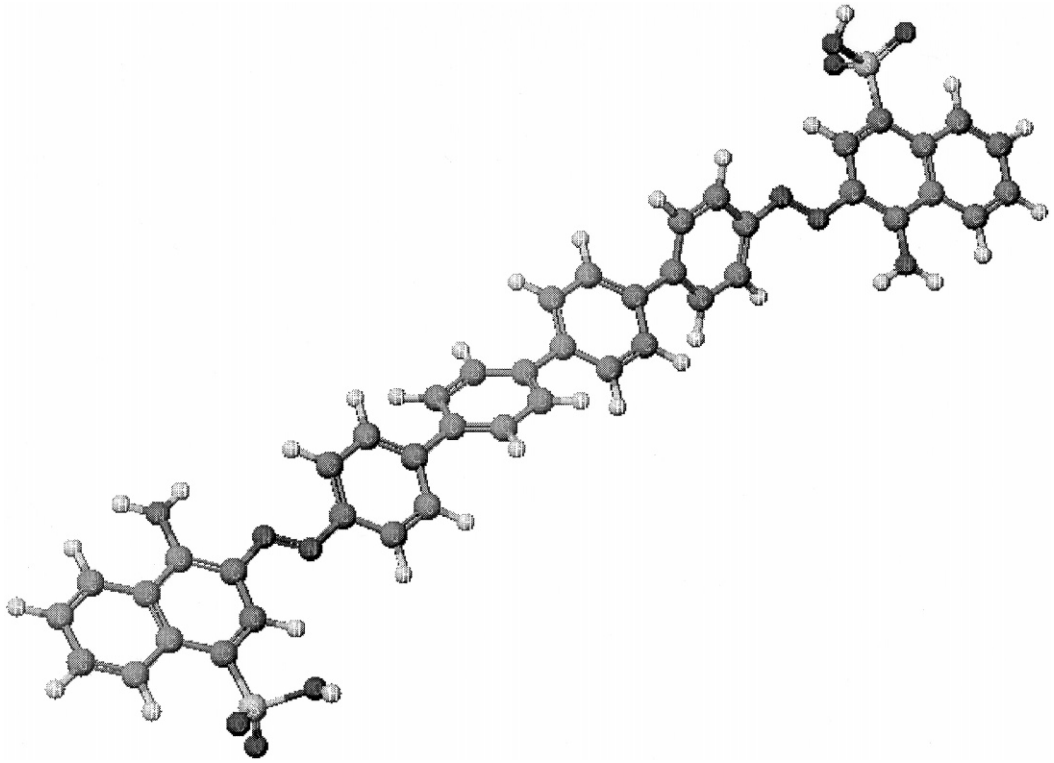

Fig. 6. Example of the result of an AM1 optimization initiated from a planar starting structure.

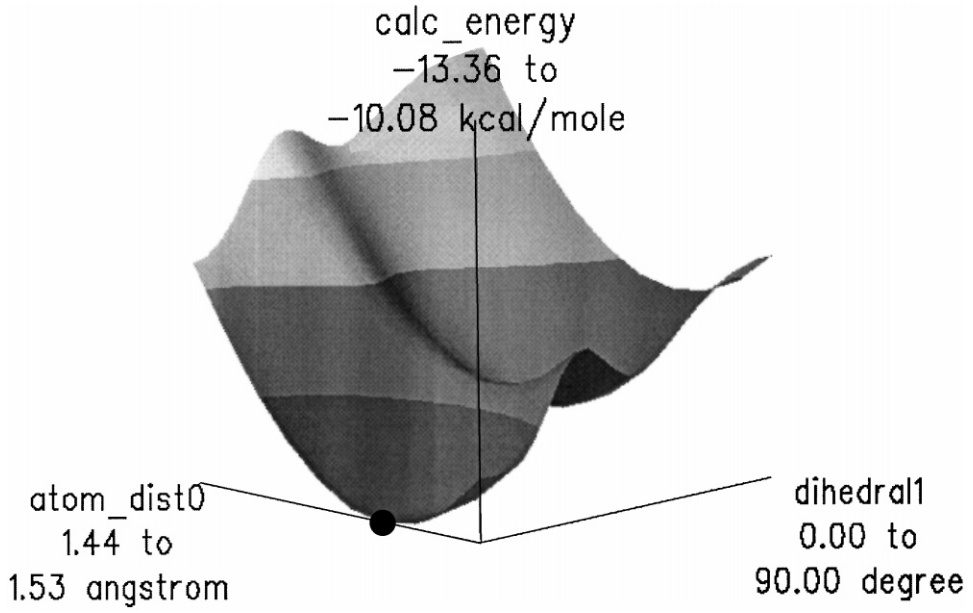

Fig. 7. PM3 conformational search map for **1**, constructed by exploring the energy changes associated with varying the length of the central phenyl–phenyl bond (“atom_dist0”), and by rotating one half of the molecule about the central phenyl–phenyl bond (“dihedral1”).

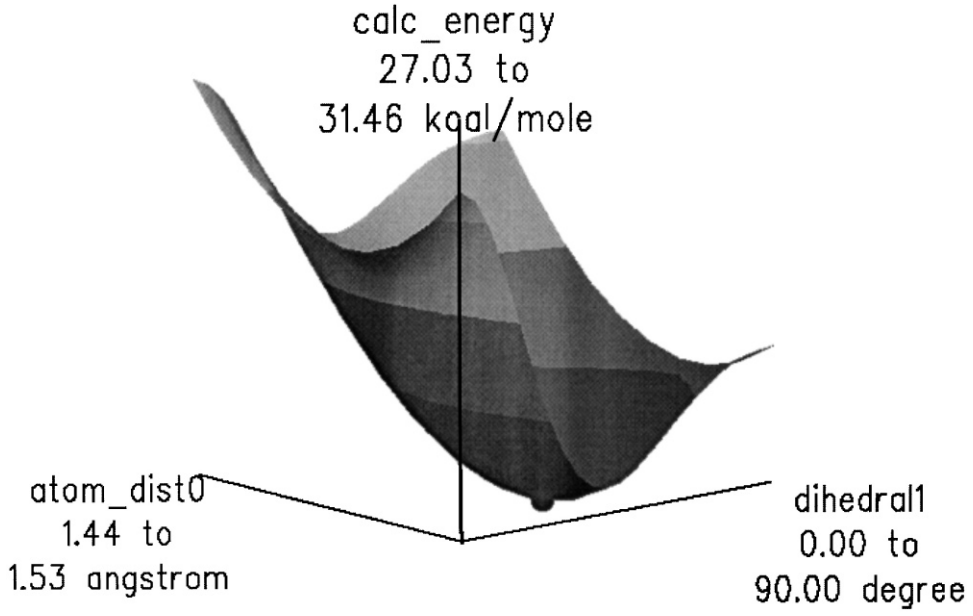

Fig. 8. AM1 conformational search map for **1**, constructed by exploring the energy changes associated with varying the length of the central phenyl–phenyl bond (“atom_dist0”), and by rotation of one half of the molecule about the central phenyl–phenyl bond (“dihedral1”).

interactions involving hydrogen atoms (including hydrogen–hydrogen interactions) at distances smaller than 2 Å [38]. As a consequence, crowded systems, such as cyclobutane and the boat conformer of cyclohexane, are predicted to be unrealistically stable by PM3 [38]. *ortho*-Hydrogen atom distances in the phenyl residues of planar conformers were predicted to differ by approximately 1.8 Å. These observations could account for the differences in AM1 and PM3 results.

3.1. Color prediction

PISYSTEM predicted that increasing the number of phenyl rings would cause a hypsochromic shift and an increase in the oscillator strength of the absorption band. PISYSTEM generates absorption intensity in terms of the oscillator strength, whereas ZINDO generates absorption intensity in terms of the magnitude of the transition moment vector (TMV) associated with the light absorption event. The two are related by:

$$\text{Oscillator strength} = \text{TMV}^2 \times \text{(average frequency of the light absorbed)}$$

Thus, as the oscillator strength or the TMV value increases, absorption intensity also increases. Although ZINDO predicted that there would not be a significant shift in λmax, it did agree with PISYSTEM concerning the increase in absorption intensity caused by increasing the number of phenyl rings. Table 3 provides a summary of the results from CAChe ZINDO and PISYSTEM.

It is clear that ZINDO was not useful for predicting the absorption spectra of dyes **1, 6, 7** and **8**, based upon the poor agreement between the experimental and predicted values for dye **1** (Congo Red). However, we found good agreement between the experimental and values using PISYSTEM.

4. Conclusions

PM3 and AM1 differed in their ability to predict the structures of Congo Red and its terphenyl and quarterphenyl analogs. PM3 predicted the central phenyl rings of such structures to be coplanar, while AM1 predicted that the central phenyl rings have a staggered arrangement, in which the angles between the planes of the central phenyl rings would be about 40°. In either case, it appears that the planar conformation is easily accessible for the terphenyl and quarterphenyl analogs, suggesting that the new dyes would have good affinity for cellulosic substrates.

The results of this study showed that increasing the number of phenyl rings in Congo Red leads to increased molar absorption intensity along with hypsochromic shifts. In this regard, PISYSTEM was more effective than ZINDO in predicting absorption spectra.

References

[1] Society of Dyers and Colourists. Colour index international. 3rd ed. CD ROM version Bradford: SDC, 1996.
[2] Prival MJ, Bell SJ, Mitchell VD, Peiperl MD, Vaughan VL. Mutagenicity of benzidine and benzidine-congener dyes and selected monoazo dyes in a modified salmonella assay. Mutat Res 1984;136:33–47.
[3] Calogero F, Freeman HS, Esancy JF, Whaley WM. An approach to the design of non-mutagenic azo dyes: 2. Potential replacements for the benzidine moiety of some mutagenic azo dyestuffs. Dyes and Pigments 1987;8:431–47.
[4] Hartman CP, Fulk GE, Andrews AW. Azo reduction of trypan blue to a known carcinogen by a cell-free extract of a human intestinal anaerobe. Mutat Res 1978;58:125–32.
[5] Reid TM, Morton KC, Wang CY, King CM. Conversion of congo red and 2-azoxyfluorene to mutagens following in vitro reduction by whole-cell rat cecal bacteria. Mutat Res 1983;117:105–12.
[6] Reid TM, Morton KC, Wang CY, King CM. Mutagenicity of azo dyes following metabolism by different reductive/oxidative systems. Environ Mutagen 1984;6:705–17.
[7] Balzarini J, Mitsuya H, DeClercq E, Broder S. Comparative inhibitory effects of suramin and other selected compounds on the infectivity and replication of human t-cell lymphotropic virus (HTLV-III)/lymphadenapathy-associated virus (LAV). Int J Cancer 1986;37:451–7.
[8] Brinkworth RI, Fairlie DP. Non-peptidic anti-AIDS agents: inhibition of HIV-1 proteinase by disulfonates. Biochem Biophys Res Commun 1992;188:624–30.
[9] Caughey B, Race RE. Potent inhibition of scrapie-associated prp accumulation by congo red. J Neurochem 1992;59:768–71.
[10] Caughey B, Ernst D, Race RE. Congo red inhibition of scrapie agent replication. J Virol 1993;67:6270–2.
[11] Turnell WG, Finch JT. Binding of the dye congo red to the amyloid protein pig insulin reveals a novel homology

against amyloid — forming peptide sequences. J Mol Biol 1992;227:1205–23.
[12] Freeman HS, Hinks D, Esancy JF. Genotoxicity of azo dyes: bases and implications. In: Peters AT, Freeman HS, editors. Physico-chemical principles of color chemistry (Vol. 4 of Advances in Color Chemistry Series). New York, London: Publ. Blackie, 1996. p. 254–92.
[13] Ojala WH, Ojala CR, Gleason WB. The X-ray crystal structure of the sulfonated azo dye congo red, a non-peptidic inhibitor of HIV-1 protease which also binds to reverse transcriptase and amyloid proteins. Antiviral Chemistry and Chemotherapy 1995;6(1):25–33.
[14] Carreira LA, Towns TG. Raman spectra and barriers to internal rotation: biphenyl and nitrobenzene. J Mol Struct 1977;41:1–9.
[15] Bastiansen O, Samdal S. Structure and barrier to rotation of biphenyl derivatives in the gaseous state. J Mol Struct 1985;128:115–25.
[16] Charbonneau G, Delugeard Y. Structural transitions in polyphenyls. iii. Crystal structure of biphenyl at 110 K. Acta Cryst 1979;B 32:1420–3.
[17] Charbonneau G, Delugeard Y. Biphenyl: three dimensional data and structural refinement at 298 K. Acta Crystall 1977;B 33:1586–8.
[18] Brock CP, Minton RP. Systematic effects of crystal-packing forces: biphenyl fragments with H atoms in all four ortho positions. J Am Chem Soc 1989;111:4586–93.
[19] Baudour PJL, Delugeard Y, Cailleau H. Transition structurale dans les polyphenyles. i. Structure cristalline de la phase basses temperature du *p*-terphenyle a 113 K. Acta Cryst 1976;B 32:150–4.
[20] Baudour PJL, Cailleau H, Yelon WB. Structural phase transition in polyphenyls. ii. Double-well potential in the disordered phase of *p*-terphenyl from neutron (200 K) and X-ray (room temperature) diffraction data. Acta Cryst 1977;B 33:1773–80.
[21] Baudour PJL, Toupet L, Delugeard Y, Ghemid S. Transitions de phase structurales dans les polyphenyles. ix. Affinements des structures du *p*-terphenyle hydrogene a 200 K (diffraction des rayons x) et du biphenyle deutere a 40 K (diffraction des neutrons. Acta Cryst 1986;C 42:1211–7.
[22] Delugeard Y, Desuche J, Baudour JL. Structural transition in polyphenyls. ii. The crystal structure of the high-temperature phase of quarterphenyl. Acta Crystall 1976;B 32:702–5.
[23] Hanssen J, Lüttke W. Verbesserte cndo/2-konformationsberechnungen konjugierter moleküle. J Mol Struct 1979;55:165–81.
[24] Momicchioli F, Baraldi I, Bruni MC. A new indo-type procedure for conjugated non-rigid molecules. i. Ground-state conformations and barriers to internal rotation. Chem Phys 1982;70:161–76.
[25] Tsuzuki S, Tanabe K. Ab initio molecular orbital calculations of the internal rotational potential of biphenyl using polarized basis sets with electron correlation correction. J Phys Chem 1991;95:139–44.
[26] Lye J, Freeman HS, Singh P, Mason ME, Hinks D. Molecular modeling in dye chemistry: studies involving two disperse dyes. Textile Res J 1999;69(8):583.
[27] CAChe Worksystem, CAChe Scientific (Oxford Molecular).
[28] Dewar MJS, Zoebisch EG, Healey EF, Stewart JJP. AM1: a new general purpose quantum mechanical molecular model. J Am Chem Soc 1985;107:3902–9.
[29] Stewart JJP. Optimization of parameters for semiempirical methods. i. Method. J Comp Chem 1989;10(2):209–20.
[30] Stewart JJP. Optimization of parameters for semiempirical methods. ii. Applications. J Comp Chem 1989;10(2):221–64.
[31] Bacon AD, Zerner MC. An intermediate neglect of differential overlap theory for transition metal complexes: Fe, Co and Cu chlorides. Theoret Chim Acta (Berl) 1979;53:21–54.
[32] Anderson WP, Edwards WD, Zerner MC. Calculated spectra of hydrated ions of the first transition metal series. Inorg Chem 1986;25:2728–32.
[33] Naef R. PISYSTEM V3.1, Im Budler6, CH-4419. Lupsingen, Switzerland, 1994.
[34] Pariser R, Parr RG. A semi-empirical theory of the electronic spectra and structure of complex unsaturated molecules: I. J Chem Phys 1953;21:466–71.
[35] Pariser R, Parr RG. A semi-empirical theory of the electronic spectra and structure of complex unsaturated molecules: II. J Chem Phys 1953;21:767–76.
[36] Pople JA. Electronic interaction in unsaturated hydrocarbons. Trans Faraday Soc 1953;49:1375–85.
[37] Redington RL, Bock CW. MO study of singlets, triplets, and tunneling in tropolone. i. Geometries, tunneling and vibrations in the ground electronic state. J Phys Chem 1991;95:10284–94.
[38] Huang W. Communication via computational chemistry list. (October 1995), Archive URL: http://ccl.osc.edu/chemistry.html.